




Real-time FPGA based simulator enabled Hardware-In-the-Loop for fuzzy control dual-sources HESS

Hatim Jbari*[‡], Rachid Askour**, Badr Bououlid Idrissi***

*Modelling, Information Processing and Control Systems (MPICS), National High School of Arts and Crafts, Moulay Ismail University, Meknes, Morocco

**Modelling, Information Processing and Control Systems (MPICS), National High School of Arts and Crafts, Moulay Ismail University, Meknes, Morocco

***Modelling, Information Processing and Control Systems (MPICS), National High School of Arts and Crafts, Moulay Ismail University, Meknes, Morocco

(ha.jbari@edu.umi.ac.ma, r.askour@umi.ac.ma, b.bououlid@umi.ac.ma)

[‡]Corresponding Author; Hatim Jbari, National High School of Arts and Crafts, Moulay Ismail University, B.P. 15290 EL Mansour Meknes 50500, Morocco, Tel: +212 662 117 122, ha.jbari@edu.umi.ac.ma

Received: 03.04.2022 Accepted: 02.05.2022

Abstract- In this paper, a Hardware-In-the-Loop (HIL) platform based real-time simulation, of a hybrid energy storage system (HESS) control is proposed. The energy management strategy (EMS) is developed using a fuzzy logic controller (FLC), designed and evaluated via software simulations, and embedded on a Field Programmable Gate Array (FPGA) platform. The HESS is built upon a fully active parallel topology, including a Li-ion battery considered as the primary source, and a supercapacitor (SC) used as the secondary source. The objective of this work is to evaluate initially, the performance of the proposed EMS, secondly, the validation of the FLC-EMS C code, developed and embedded in the NIOS II Core of FPGA's Altera type. The validation of the developed code is performed by comparing the results obtained via the HIL with those of the software simulation. The HIL simulations of the proposed model and strategy were performed using MATLAB/SIMULINK, under ECE-15 cycle.

Keywords Electric vehicle, FPGA, Fuzzy Logic Controller, Hardware-In-the-Loop, Hybrid Energy Storage System.

1. Introduction

Nowadays, global warming is a major priority of all the world's concerns. Environmental Organisations and automotive manufacturers combine their efforts and investments, to reduce the impact and greenhouse gas emission rates of ground transportation [1]. The deployment of zero-emission vehicle (Z-EV) projects, or pure electric vehicles (P-EV), provides a technological solution with benefits for environment and global health [2, 3], especially in urban areas. Indeed, scientists work intensively on this solution to enable this vehicle typology to consolidate its place in the low-CO₂-emission vehicle segment. The inclusion of P-EV challenges developers to overcome its limitations, particularly those related to the electric machine-based powertrain, battery-based energy storage system capacity [4, 5], and performance of battery chargers [6], related to their efficiency, regulation and quality of supplied power.

Batteries are characterised by a high energy density. However, this energy storage device, considered as a main source in a P-EV, presents the disadvantage of having a low power density and a limited lifespan. The battery's performance is affected by high number of charge-discharge cycles [7, 8], and fast power demands [9]. However, other electrical energy storage systems provide energy performance that allows to overcome the limitations of batteries, such as supercapacitors (SC). It can be used as a complementary storage system to batteries, creating a Hybrid Energy Storage System (HESS). According to [10], the development of a HESS powering an EV, increases the performance of power supply system, and optimises the lifespan of battery by reducing its stress. Moreover, the HESS allows a complementarity of instantaneous power demands [11], and the possibility to provide a large energy supply for an extended range. In addition, the adequate topology of the HESS should be adopted to improve the system's energy efficiency. Indeed,

a comparative study of different topologies efficiency has been conducted in [12-14], based on the complexity of the architecture, the type and number of converters, the control and stability of the DC voltage supplying the machine, and the system efficiency. Another issue of EV performance improvement has been elaborated in [15], aiming at an optimal design of charging stations for charging and discharging EVs in a smart grid environment, based on Priority Based Algorithm (PBA).

The energy management system (EMS) is a key element that allows to overcome the batteries limitations. The objective of the EMS is to ensure an optimised energy distribution between the HESS sources (SCs and battery). In [16], an EMS based on adaptive fuzzy controller is developed for an HESS's active topology, based on SCs and battery. The EMS takes into consideration the criteria of SC's State of Charge (SoC) difference between the beginning and the end of each cycle, the total energy conversion chain efficiency and the battery current variation, in order to evaluate the performance of the developed strategy. The architecture and objectives mentioned previously have been used in [17], in addition to the RMS current and battery load minimisation, which are considered as objectives, and represent factors that increase the battery degradation. An EMS based on a classical FLC was presented in [18] to ensure an efficient energy split in an architecture like that previously mentioned in [17]. This work presents an EMS that uses three cascaded FLCs. The first one is designed to control the power supplied by SCs and battery, taking into consideration SoC of both sources and battery lifespan. The second and third FLC are used to provide duty cycle to control the DC-DC converters. The FLC inputs references are the powers differences, generated by the first FLC. Another work presented in [19], aims to develop a fuzzy sliding mode-based strategy designed for the control of multiphase and interleaved bidirectional DC-DC converters, for EV applications. The objective of this work is to increase the high voltage performance, to ensure a more efficient control and an equal sharing of the load current between each converter module.

Currently, the development cycle of all industrial sectors is governed by the time-to-market and the system complexity. Hardware-In-The Loop (HIL) solution provides a perfect opportunity to satisfy these challenges, for the development of critical control applications, particularly for EV's control system design. HIL simulation can provide an effective solution to the imperfections of traditional methods. For this purpose, a variety of solutions have been developed, e.g., MATLAB/Simulink for software application, Digital Signal Processor (DSP) [20-21] as an interface and FPGA [22-25] as a processor controller system. A second application of the HIL was performed in [26], which consists in performing a co-simulation (HIL) to conduct a quick verification of the developed algorithm, embedded on a ZYBO-27 FPGA platform, which controls a motor via a power converter, emulated on a TYPHOON HIL 402 real time platform. Thus, the HIL reduces the risk, cost and time required to evaluate complex embedded systems.

This paper proposes a HIL simulation of a 1.5 kW HESS based on an active topology. The EMS uses a FLC-based rules controller. The HESS model was developed in a previous work detailed in [17]. The EMS algorithm was developed and embedded on an ALTERA Cyclone IV FPGA as a C code, executed by the NIOS II core. The objective of this work is to evaluate the performance of the EMS and validate in real time the developed C code algorithm, by comparing the HIL results with those of the simulation.

The rest of this paper is organised as follows: section 2 presents a description of the proposed model and the developed EMS. Section 3 details the developed HIL. Section 4 discusses the results of the experimentation and simulation. Finally, Section 5 concludes the paper.

Nomenclature

C_{SC}	SC Capacitance (F)
COG	Center Of Gravity
E_{bat}	Battery energy
EMS	Energy Management System
FPGA	Field Programmable Gate Array
HESS	Hybrid Energy Storage System
HIL	Hardware-In-the-Loop
i_{bat}	battery current (A)
i_{bat_ref}	battery current reference (A)
i_{ch_bat}	DC-DC battery Current converter (A)
i_{ch_sc}	DC-DC SC Current converter (A)
i_{DC}	DC BUS Current (A)
I_{reg_max}	Maximum current regenerated by braking
i_{req_ref}	HESS Current reference (A)
i_{sc}	SC current (A)
i_{sc_ref}	SC current reference (A)
k_{cont}	Battery contribution factor
M_{bat}	Battery mass
M_{SC}	SC mass
N_{bat}	Number of Battery Cells in series
N_{sc}	Number of SC Cells in series
P_{bat_Fil}	Filtered battery power reference
P_{bat_lim}	Battery power limit
P_{req}	Required drivetrain power (W)
R_{ESR}	SC Equivalent Series Resistance
RMSD	Root Mean Square Deviation
SC	SuperCapacitors
SoC_{sc}	SC State of Charge (%)
U_{bat}	battery voltage (V)
U_{bat_meas}	Measured battery voltage (V)
U_{DC}	DC BUS voltage (V)
U_{ch_bat}	DC-DC battery voltage converter (V)
U_{ch_SC}	DC-DC SC voltage converter (V)
U_{sc}	SC voltage (V)
ρ_{bat}	Battery energy density
η_p	Power ratio

2. Proposed HESS and energy management strategy

2.1. HESS Presentation

The studied system (Figure 1) is a HESS based on an active topology, which provides a maximum power of 1.5kW, using a Li-ion battery and SCs as power sources. The proposed HESS is equipped with two converters to control the battery and SCs separately, which allows a flexible power management, and provides the possibility to be easily scaled up to other required power value.

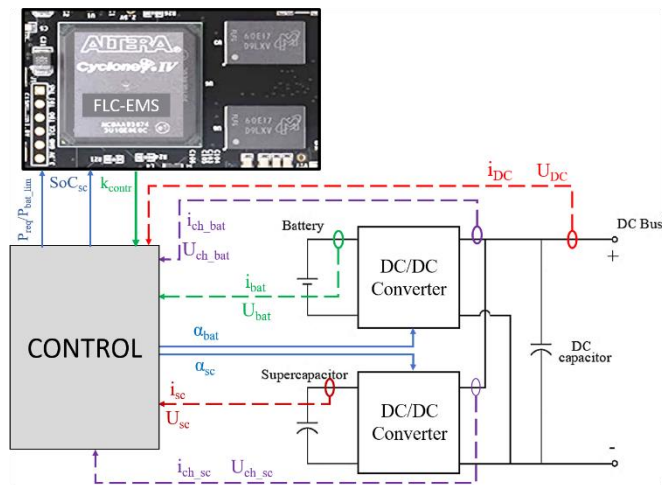


Fig. 1. Synoptic scheme of the studied HESS.

Table 1. Li-ion Battery (3.7V Lithium cells)

Variables	Symbol	Value	Unit
SoC Limits	SoC_{bat}	[30, 100]	%
Cells in series	N_{bat}	7	-
Energy density	ρ_{bat}	160	Wh/kg
Battery mass	M_{bat}	7.5	Kg
Battery energy	E_{bat}	50	Ah
Power limit	P_{bat_lim}	1.5	kW

Table 2. Supercapacitors (SCP0650C0-0002R7STA - 650F, 2.7V, SPSCAP)

Variables	Symbol	Value	Unit
SoC Limits	SoC_{SC}	[50, 100]	%
Cells in series	N_{SC}	13	-
ESR	R_{ESR}	0.8	mΩ
SC mass	M_{SC}	10.335	Kg
Cell Capacitance	C_{SC}	650	F

Therefore, the modelling and control of the studied system has been performed using the EMR approach [27-28] in a previous work presented in [17]. The same model is adapted for a 1.5 kW maximum power demand, to ensure a constant voltage of the DC BUS $U_{DC}=24V$, and validate the EMS developed and embedded in the FPGA using HIL

simulation. The characteristics of the Li-ion battery and SCs used in this study are presented in Table 1 and Table 2.

2.2. Proposed Energy Management System

The present study aims at improving the real-time energy management of the proposed dual-source HESS (SCs, battery). The developed EMS shown in Figure 3, is designed to make decisions that assure the optimized contribution of each HESS source. The most important objective of EMS implementation is to satisfy the power demand, respecting criteria related to battery power limit, battery stress reduction, and available energy in SCs.

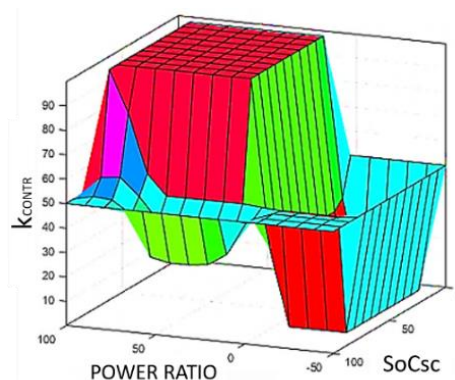


Fig. 2. Output Battery's contribution.

Then, the proposed approach based on FLC-EMS for real time decision making, should assure a power profile with a maximum value of 1.5kW, that represents the battery power limit P_{bat_lim} , and the control of SCs in an optimal range $SoC_{SC} \in [50\%, 100\%]$ during each cycle, in order to make it able to satisfy the power requirements of the next cycle. Then, the following rules should be respected:

➤ The power requirements P_{req} is negative: the recovered power is supported by SCs during transient phases, specifically the power pulses. Once the SCs are completely charged, the quasi-constant low frequency component of the recovered power is supported by battery.

➤ The power requirements P_{req} is positive: the power demand during the transient phase should be supported by SCs (when: $P_{req} < P_{bat_lim}$ and $SoC_{SC} \in [50\%, 100\%]$), specifically the power pulses. The quasi-constant power demand is supported by battery.

Thus, according to the theoretical basis of fuzzy logic control, which consists to process imprecise parameters on continuous values ranged from 0 to 1, the output value depends on the degree of membership of a satisfied condition. The proposed fuzzy controller supports two input groups ($P_{req}/P_{bat_lim}, SoC_{SC}$), and one output group k_{cont} that defines the battery's contribution. The processing consists of three important steps: fuzzification, inference rules processing and defuzzification.

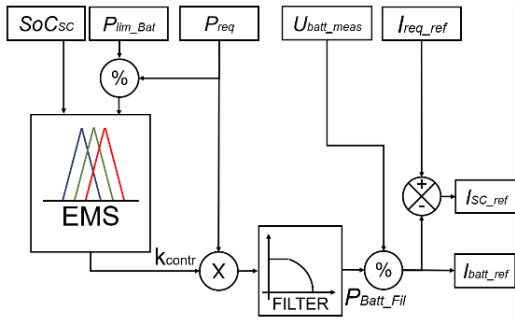


Fig. 3. EMS Strategy [17].

Fuzzification is the first step in fuzzy processing. It defines the linguistic variables and the membership functions of the FLC inputs. The fuzzy system applied to the proposed model, includes two input variables: SoC_{SC} and the power ratio (P_{req}/P_{bat_lim}) (Figure 4). Thus, three membership groups have been defined for SoC_{SC} : LOW_SC_CHRG, MED_SC_CHRG and HIGH_SC_CHRG which represent the SCs charging level. For the second input variable: P_{req}/P_{bat_lim} , three membership groups have been defined, which represent the ratio level of the required power to the battery power limit: LOW_PWR, MED_PWR and HIGH_PWR.

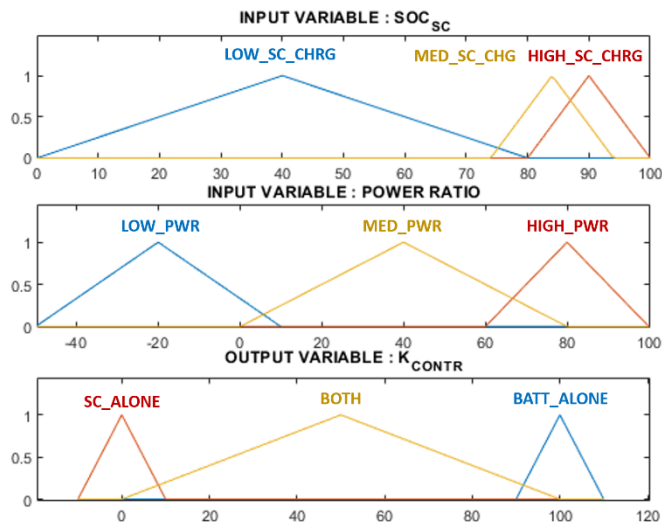


Fig. 4. EMS membership functions.

The inference process is the second step of the fuzzy approach (Figure 4). It aims at deducing the output variable state, according to the knowledge of the input variable's state. In this case, the inference engine contains nine rules that include all possible combinations (Table 3), i.e., IF "power demand is medium" AND "the state of charge of the supercapacitor is high" THEN "the contribution is that of the supercapacitor alone".

Table 3. Rules-base of Fuzzy Logic Controller

	LOW_SC _CHRG	MED_SC _CHRG	HIGH_SC _CHRG
LOW_PWR	SC_ALONE	BOTH	BOTH
MED_PWR	BATT_ALONE	BOTH	SC_ALONE
HIGH_PWR	BATT_ALONE	BOTH	BOTH

Defuzzification is the last step of the fuzzy processing, which aims to calculate the output variable k_{cont} (Figure 2), represented by the centroid abscissa of the output resulting fuzzy area (Mamdani approach). In fact, three membership groups have been defined (SC_ALONE, BOTH, BATT_ALONE) that represent the battery contribution level. Thus, the resulting fuzzy rules (surface of possible decisions) according to the SoC_{SC} variations and the load power demand value, allows to define the current supplied by battery through a filtered current reference (Figure 3).

3. Hardware-In-The-Loop Development

A simulation, is a scientific approach that explores hypothesis through digital computation [7]. Therefore, in order to evaluate a theoretical design model, a software environment is used to simulate characteristics and subsystem interactions. However, the real-time HIL simulator, is a software-hardware platform, designed for complete diagnosis of a control system. This technology is used to evaluate the performance of a real control electronic unit, via the obtained results instead of using conventional hardware (e.g., Oscilloscope).

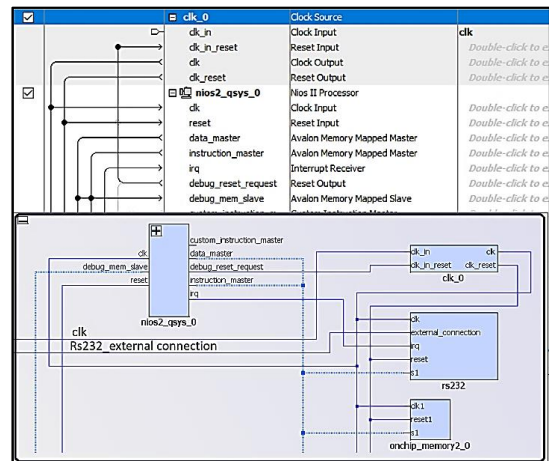


Fig. 5. Altera Qsys interface and NIOS II processor configuration options scheme.

The objective of this section is to present a system integration platform, to build a HIL real-time simulator, using the proposed HESS model developed with MATLAB/SIMULINK. Indeed, the Altera Cyclone IV FPGA chip and the Qsys integration tool are used (Figure 5).

The NIOS II processor soft core is available with Altera's tools. Therefore, the designed FLC-EMS algorithm, is programmed using the C language and implemented in the NIOS II FPGA's processor core. The experimentation is performed on the ALTERA Cyclone IV EP4CE6 FPGA Development Board (Figure 6).

The built system includes the following elements:

- A NIOS II processor in a basic configuration;
- A UART (Universal Asynchronous Receiver Transmitter) for serial communication with MATLAB simulation platform through USB port;

- A memory that uses the internal NIOS II ON-chip memory blocks;
- The MAX232 circuit on the development board, which is used as an interface between a TTL serial link (0-5V) on the FPGA board, and the RS232 serial link;
- A RS232 to USB converter that enables the communication with FPGA, and control of the simulation model in MATLAB/SIMULINK. The Figure 7 shows the structure of the described system.

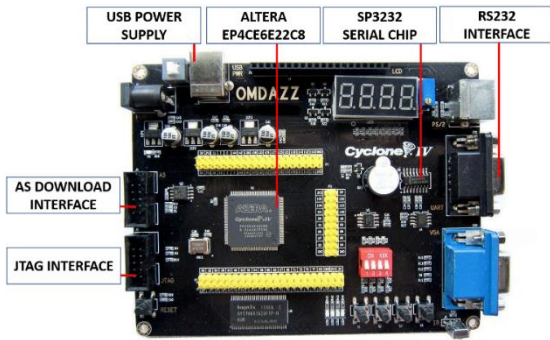


Fig. 6. ALTERA Cyclone IV EP4CE6 FPGA Development Board.

The proposed FLC-EMS is based on Mamdani's inference mechanism [25], to build and execute the fuzzy rules. The scheme presented in Figure 8 explains the functionalities of the developed program, executed by the NIOS II core of the FPGA hardware platform.

In the first step, the values of the input variables (SoC_{SC} , $\eta_p = P_{req}/P_{lim_bat}$) are sent by the MATLAB/SIMULINK model platform via serial port, received by the NIOS II processor core. This operation is achieved by the first part of the code which assures the concatenation of the 8 bits data and its conversions to the "Float" value type.

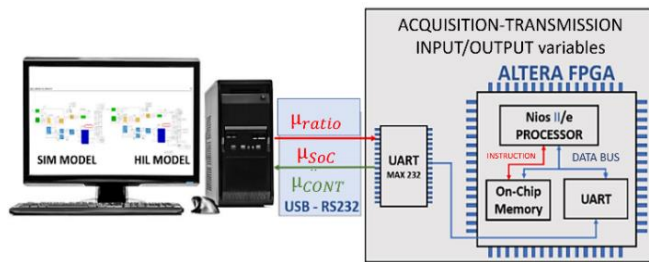


Fig. 7. Scheme of the developed EMS HIL.

➤ **Fuzzification**

Fuzzification is the second step of the developed EMS algorithm, which transforms the numerical inputs (SoC_{SC} , $\eta_p = P_{req}/P_{lim_bat}$) into a membership set in the range of [0,1], to corresponding fuzzy sets α_j (j is an index which defines the desired input: $j=1$ for $\eta_p = P_{req}/P_{lim_bat}$ and $j=2$ for SoC_{SC}). The membership function (MF) is a triangular function, which defines the value of the membership degree of each input. Indeed, each input is described by three MFs. These last are defined by three vertices of a triangle: $I_{i,j}$, $I_{i+1,j}$ and $I_{i+2,j}$ where i is an index which indicates the number of the point $I_{i,j}$ (Figure 8). The coordinates of $I_{i,j}$ are noted $X_{i,j}$ and $Y_{i,j}$.

The fuzzification mechanism shown in Figure 8, proceeds first to the determination of the universe of discourse for each input variable (i.e., the range of values that the variable can take). Then, the degree of membership is defined according to the membership interval of the input variable: $[I_{i,j}, I_{i+1,j}]$. A function (ranging from 0% to 100%) is used to define the proportion of truth for each variable, it's described by the equation of the triangle function (1):

$$\mu_{k,j}(\alpha_j) = \frac{(Y_{i+1,j} - Y_{i,j})}{(X_{i+1,j} - X_{i,j})} \alpha_j + (Y_{i,j} - \frac{(Y_{i+1,j} - Y_{i,j})}{(X_{i+1,j} - X_{i,j})} X_{i,j}) \quad (1)$$

where k is an index of the MF adopted ($k \in [1,2,3]$).

➤ **Construction of Inference rules**

Based on the operations previously performed, a series of rules are implemented. Each rule allows to define the response through a decision matrix presented in Table 4, according to the defined fuzzy rule of the following formula (2):

$$\text{IF } \mu_{k,1}(\alpha_1) \text{ IS A AND } \mu_{m,2}(\alpha_2) \text{ IS B THEN } \gamma_{k,m} \text{ IS C} \quad (2)$$

where k and m are respectively the indexes of the MF adopted for the inputs η_p and SoC_{SC} .

The "AND" operator in fuzzy logic approach, is equivalent to the minimum operation. The application of this operator to $(\mu_{k,1}(\alpha_1), \mu_{m,2}(\alpha_2))$, generates the function $\gamma_{k,m}(\mu_{k,1}, \mu_{m,2})$ representing the input MFs intersection.

A truth set for each rule is then calculated. The construction of these rules is principally based on "AND" operator. Indeed, the code implemented in the NIOS II core is mathematically based on formulas shown in (3).

$$\begin{cases} \gamma_{k,m} &= \min(\mu_{k,1}(\alpha_1), \mu_{m,2}(\alpha_2)) \\ \gamma_{SC_Alone} &= \min(\gamma_{1,1}, \gamma_{2,3}) \\ \gamma_{Both} &= \min(\gamma_{1,2}, \gamma_{2,2}, \gamma_{3,1}, \gamma_{1,3}, \gamma_{3,3}) \\ \gamma_{Batt_Alone} &= \min(\gamma_{2,1}, \gamma_{3,1}) \end{cases} \quad (3)$$

➤ **Defuzzification**

Defuzzification is the process that convert a fuzzy value into a crisp value. Centre Of Gravity (COG) defuzzification is more frequently used. It defines the output that corresponds to the area COG of the output membership function, characterizing the fuzzy set resulting from decision-making matrix outputs. Indeed, Area and COG of each sub regions of $\gamma_{k,m}$ are calculated. Then, the calculation of the surface COG is done as follows:

$$\mu_{out} = \frac{1}{\sum_{i=1}^n S_i} (\sum_{i=1}^n (S_i X_{S_i})) \quad (4)$$

where S_i and X_{S_i} are the area and COG of i^{th} sub-region. Note that $S_i = \int \gamma_{k,m}(x) dx$ and n is the number of sub-regions.

X_{S_i} is polygon's centroid which is defined by its vertices $(x_0, y_0), (x_1, y_1), \dots, (x_{n-1}, y_{n-1})$ and described by (5):

$$X_{S_i} = \frac{1}{6A} \sum_{j=0}^{n-1} (x_j + x_{j+1})(x_j y_{j+1} - x_{j+1} y_j) \quad (5)$$

$$\text{where: } A_i = \frac{1}{2} \sum_{j=0}^{n-1} (x_j y_{j+1} - x_{j+1} y_j) \quad (6)$$

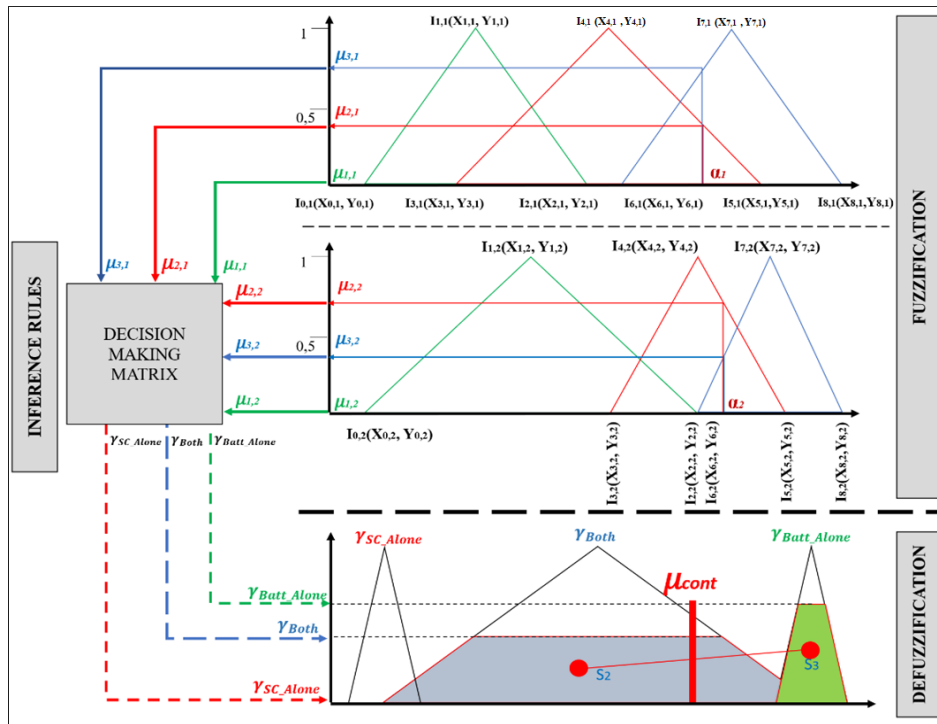


Fig. 8. Mechanism of the proposed FLC-EMS Code.

Table 4. Decision-making matrix

AND		$\mu_{1,2}$	$\mu_{2,2}$	$\mu_{3,2}$
$\gamma_{k,m} = \min(\mu_{k,1}(\alpha_1), \mu_{m,2}(\alpha_2))$		$\alpha_2 \in [I_{0,2}, I_{1,2}]$ or $[I_{1,2}, I_{2,2}]$	$\alpha_2 \in [I_{3,2}, I_{4,2}]$ or $[I_{4,2}, I_{5,2}]$	$\alpha_2 \in [I_{6,2}, I_{7,2}]$ or $[I_{7,2}, I_{8,2}]$
$\mu_{1,1}$	$\alpha_1 \in [I_{0,1}, I_{1,1}]$ or $[I_{1,1}, I_{2,1}]$	$\gamma_{1,1}(SC_Alone)$	$\gamma_{1,2}(Both)$	$\gamma_{1,3}(Both)$
$\mu_{2,1}$	$\alpha_1 \in [I_{3,1}, I_{4,1}]$ or $[I_{4,1}, I_{5,1}]$	$\gamma_{2,1}(Batt_Alone)$	$\gamma_{2,2}(Both)$	$\gamma_{2,3}(SC_Alone)$
$\mu_{3,1}$	$\alpha_1 \in [I_{6,1}, I_{7,1}]$ or $[I_{7,1}, I_{8,1}]$	$\gamma_{3,1}(Batt_Alone)$	$\gamma_{3,1}(Both)$	$\gamma_{3,3}(Both)$

Therefore, the development of the defuzzification algorithm, takes into account the criterion of processing speed as a fundamental requirement, in order to ensure a fast response of the EMS implemented in FPGA. Indeed, the defuzzification function of the developed algorithm, is designed to calculate the COG based on the mesh of the resulting polygon surface. For this purpose, the triangle model has been taken as the basic element of the generated mesh, since this model allows to simplify the calculation formulas (4) and (5). The COG of triangle model is based on the average of the vertices coordinates in the new formulas, as illustrated in equations (7), (8), (9) and Figure 9.

$$X_{Si} = \frac{1}{3}(x_j + x_{j+1} + x_{j+2}) \tag{7}$$

$$S_i = \frac{1}{2}h(x_{j+1} - x_j) \tag{8}$$

where the triangle height is expressed as following:

$$h = |y_{j+2} - y_j| \tag{9}$$

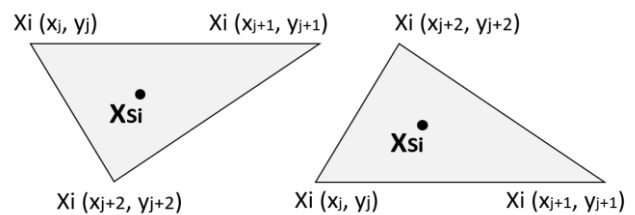


Fig. 9. Mesh triangle configurations.

After the analysis of the obtained polygons presented in Figure 10 and 11, five groups of areas were defined. The areas are activated by comparing the defuzzification inputs (γ_{SC_Alone} , γ_{Both} , γ_{Batt_Alone}), with the intersection point of the outputs triangles ($P_i(X_{Pi}, Y_{Pi})$):

➤ $S_{SC_ALONE} = (S0 \cup S1 \cup S2 \cup S9 \cup S10 \cup S11)$ depends on γ_{SC_ALONE} ;

➤ $S_{BOTH} = (S3 \cup S4 \cup S5 \cup S12 \cup S13 \cup S14)$ depends on γ_{SC_ALONE} ;

- $S_{BATT_ALONE} = (S6 \cup S7 \cup S8 \cup S15 \cup S16 \cup S17)$ depends on γ_{SC_ALONE} ;
- S2 depends on γ_{SC_ALONE} and γ_{BOTH} ;
- S6 depends on γ_{BOTH} and γ_{BATT_ALONE} .

Therefore, the calculation of the COG is performed based on the abscissas calculated from the inputs (γ_{SC_Alone} , γ_{Both} , γ_{Batt_Alone}), and the coordinates of the vertices of the MFs predefined during the development of the EMS. Thus, Table 5

summarizes the processing performed by the algorithm, to compute the areas used for the COG calculation of the resulting polygon.

Thus, the calculation of the COG surface abscissa of the resulting polygon, represents the contribution of the battery k_{cont} . This value is sent via the serial port to the simulation model platform running under MATLAB/SIMULINK, so that a new calculation loop can be started.

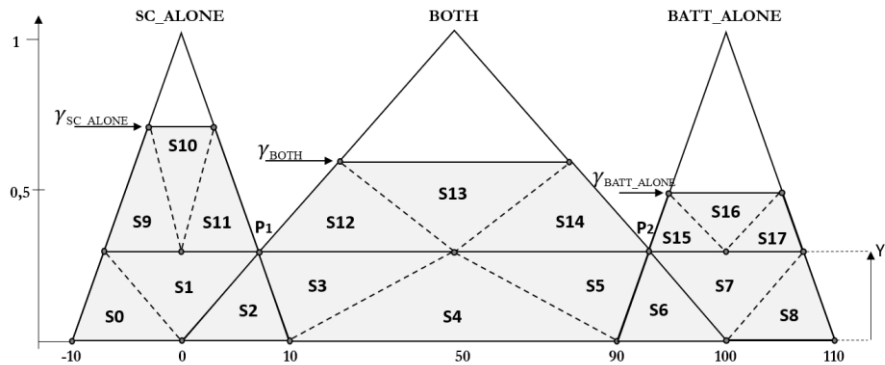


Fig. 10. Resulting polygon mesh ($\gamma_{SC_ALONE} > Y_P$, $\gamma_{BOTH} > Y_P$, $\gamma_{BATT_ALONE} > Y_P$).

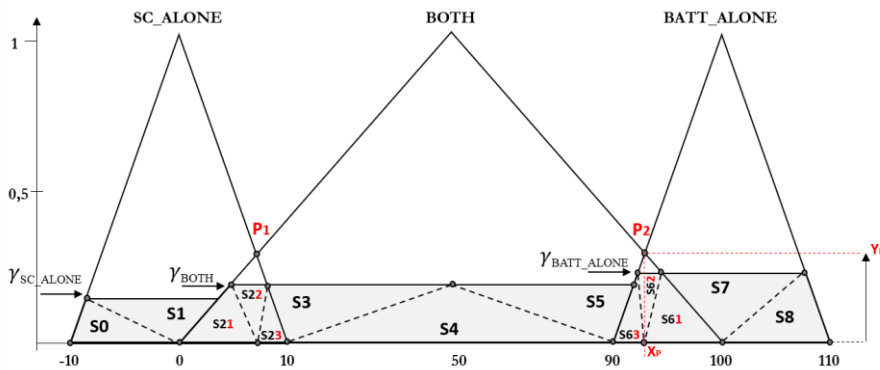


Fig. 11. Resulting polygon mesh ($\gamma_{SC_ALONE} < Y_P$, $\gamma_{BOTH} < Y_P$, $\gamma_{BATT_ALONE} < Y_P$).

Table 5. Conditions and used formulas for COG calculation

Conditions	Active Areas	
$\gamma_{SC_ALONE} > Y_P$	S0, S1, S2	$h = Y_P$
	S9, S10, S11	$h = \gamma_{SC_ALONE} - Y_P$
$\gamma_{BOTH} > Y_P$	S2, S3, S4, S5, S6	$h = Y_P$
	S12, S13, S14	$h = \gamma_{BOTH} - Y_P$
$\gamma_{BATT_ALONE} > Y_P$	S6, S7, S8	$h = Y_P$
	S15, S16, S17	$h = \gamma_{BATT_ALONE} - Y_P$
$(\gamma_{SC_ALONE} < Y_P) \ \&\&$ $(\gamma_{BOTH} < Y_P)$	S21, S22, S23	$h = \max(\gamma_{SC_ALONE}, \gamma_{BOTH})$
	S0, S1	$h = \gamma_{SC_ALONE}$
$(\gamma_{BATT_ALONE} < Y_P) \ \&\&$ $(\gamma_{BOTH} < Y_P)$	S3, S4, S5	$h = \gamma_{BOTH}$
	S61, S62, S63	$h = \max(\gamma_{BATT_ALONE}, \gamma_{BOTH})$
$(\gamma_{BOTH} < Y_P)$	S7, S8	$h = \gamma_{BATT_ALONE}$
	S3, S4, S5	$h = \gamma_{BOTH}$ (While $h = 0$: not activated by the previous function)

4. Simulation and Experimental Results

The simulation models were built and run in the same MATLAB/SIMULINK platform, and evaluated under the ECE-15 driving cycle. The first model (SIM MODEL) uses the FLC-EMS developed with SIMULINK tools. The EMS control of the second model (HIL MODEL) is provided by the FPGA via serial port, to control the battery contribution (Figure 12). As it is shown in Figure 12, the ALTERA Cyclone IV EP4CE6 FPGA development board is connected to the computer via the serial port, in order to be able to receive the data (SoC_{SC} , P_{req}/P_{bat_lim}) transmitted from the simulation model running on MATLAB/SIMULINK, and to transmit the value of k_{CONTR} in real time, as it has been described in detail in the previous section. The initial SoC_{SC} and SoC_{Bat} are 81% and 95% respectively. The objective of the simulation and experimentation is to evaluate the performance of the EMS and validate the code embedded in the FPGA, by comparing the results of the developed models (simulation and HIL).

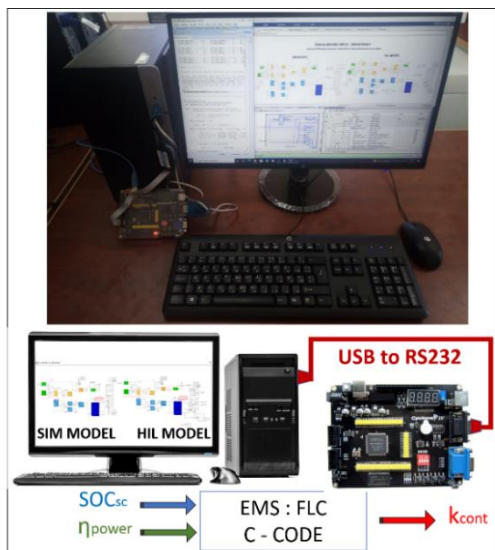


Fig. 12. Hardware-In-the-Loop (HIL) architecture for proposed HESS.

Indeed, the first evaluation criterion of the developed EMS consists in the SCs control, and ensure their functioning as an energy buffer, in the range defined during the development of the EMS: $SoC_{SC} \in [50\%, 100\%]$. The control in this range ensures an optimal energy efficiency of SCs. Thus, according to the analysis of Figure 13, both models: simulation and HIL provide very close results concerning the following parameters: SoC_{SC} , SoC_{bat} and power ratio P_{req}/P_{lim_bat} . The range of SoC_{SC} variations, doesn't exceed the interval defined in the EMS: $SoC_{SC} \in [52\%, 81\%]$, and the difference of SoC_{SC} between the initial and final state doesn't exceed 0.07% ($SoC_{SC}(t_f) - SoC_{SC}(t_i) = 0.07\%$), which demonstrates that the EMS ensures the SCs control as a perfect energy buffer.

The second evaluation criterion of the EMS, concerns the analysis of the decisions made by the EMS, particularly the management of the contributions of each energy source. Indeed, according to Figure 13 and 14, the rules defined during

the EMS development were respected during the different periods of the ECE-15 cycle:

- Negative power (braking): The SCs are engaged by EMS to support the power generated during these temporary phases: [23, 26]s, [85, 94]s and [175, 187]s. This power, which is represented by a negative current in Figure 14, is relatively high in current value ($I_{reg_max} = 41.12A$). The energy recovered during this phase is exploited in the SCs recharging, which is useful for this device, to make it able to satisfy the next reuse.

- Constant and quasi-constant power demand: During this temporary phase, the EMS ensures that battery can supply constant and quasi-constant power during the following time intervals: [14, 23]s, [60, 85]s and [142, 175]s. The minor variations in power demand have a limited impact on the battery's performance, which reduces the stress on the battery and improves its reliability.

- Positive power (power pulses): this phase is very important, as the EMS is expected to make the SCs contributing to support 60% to 90% of power pulses on one hand, and the battery to support progressively the remaining energy on the other hand during : [10, 14]s, [50, 60]s and [116, 142]s. Figure 14 demonstrates the reliability of the EMS decision making, by exploiting the fast dynamics characteristic of SCs, to satisfy the high current requirements during a short period of time, and the minimisation of the high and fast current demand impact on battery degradation. This demonstrates the advantage of SCs integration.

The third evaluation criterion of the developed EMS, is the reduction of the battery charge/discharge cycles, without compromising the constant value of DC bus voltage, respecting the battery power limit. According to Figure 13, the profile of the SoC_{batt} is smoothed, and the frequency of the battery current variation is minimal compared to that of the SCs shown in Figure 14.

Moreover, Figure 15 shows that the DC bus voltage is almost constant: $U_{DC} = 24V$ during the ECE-15 cycle, which shows that the complementarity between the HESS's energy sources is optimal, and the EMS's decision making is of high performance. On the other hand, the battery power ratio shown in Figure 13 does not exceed $P_{req}/P_{lim_bat} < 1$. The observed maximum value is $P_{req}/P_{lim_bat} = 0.96$.

The experimental results allow to validate the developed EMS code and provide perspectives on a better integration in a hardware control platform, designed for a dual source HESS. Indeed, according to Figure 13, 14 and 15, the sources $SoCs$, currents (battery and SCs) and DC BUS voltage curves profiles are almost similar (simulation and HIL results). Thus, the EMS embedded in the FPGA operates appropriately to the input's variations (SoC_{SC} , P_{req}/P_{bat_lim}) in the same way as the SIMULINK block. Thus, the EMS algorithm embedded in the FPGA seems to work correctly.

The obtained results by HIL and simulation models, allow to observe an acceptable registered error. Indeed, according to the results analysis shown in Table 6, precisely, the Root Mean Square Deviation (RMSD) between HIL and SIMULINK model energetic parameters. They seem to be weakly affected,

as they register an accepted RMSD values. The origin of this values is the result of the precision fixed in the code compiled by the NIOS II core, which has a value of $1e-3$. The error value was set to ensure optimal performance of the simulation time, and the data transfer speed between the simulation platform and the FPGA, via serial port. Thus, the simulation results show that the algorithm embedded on the FPGA is completely functional.

Table 5. Registered RMSD and Maximum error (HIL-Simulation)

Parameters	RMSD	Error _{max}
SoC_{SC} (%)	0.0246	0.056
SoC_{Bat} (%)	10^{-4}	$2.28 \cdot 10^{-4}$
I_{SC} (A)	0.0256	0.0744
I_{Bat} (A)	0.0264	0.0745
U_{DC} (V)	$3.12 \cdot 10^{-6}$	$8.9 \cdot 10^{-5}$
P_{req}/P_{lim_batt}	$3.1474 \cdot 10^{-17}$	$3.33 \cdot 10^{-16}$

5. Conclusion

In this paper, a HIL solution has been presented, aiming at the validation of an FLC-based EMS algorithm. The proposed EMS has been developed using C code and embedded on an ALTERA FPGA. The objective of the proposed EMS development is to ensure the control of an active topology HESS.

The results of the simulation and the HIL experimentation, demonstrate on the one hand, that the

developed EMS with a fuzzy logic controller, satisfies perfectly the requirements fixed during its development related to:

- SCs integration and control as an energetic buffer;
- Battery charge/discharge cycles reduction;
- Battery power limit;
- Robustness of the EMS decision-making, related to the activation of each source, depending on the different driving cycle phases (acceleration, constant speed and braking).

On the other hand, the algorithm developed and executed on the NIOS II FPGA core, is functional and in perfect agreement with the EMS based on the SIMULINK block, as demonstrated by the obtained RMSD values. The obtained results allow to validate the theoretical bases of the fuzzy logic approach and the FLC-EMS C code embedded in the FPGA.

The presented approach has been validated for an FLC based EMS, using nine rules and three MFs for the designed inputs/outputs. Moreover, the UART is used as a FPGA communication interface, which imposes a very important simulation time. Therefore, future work will focus on the development of an EMS based on the same controller, adopting a more complex algorithm with a number of MFs exceeding three functions. The hardware implementation will apply the same approach presented and explained in this article. The validation of the EMS will be performed using a faster interface like dsPACE, and other hardware platforms like the STM32.

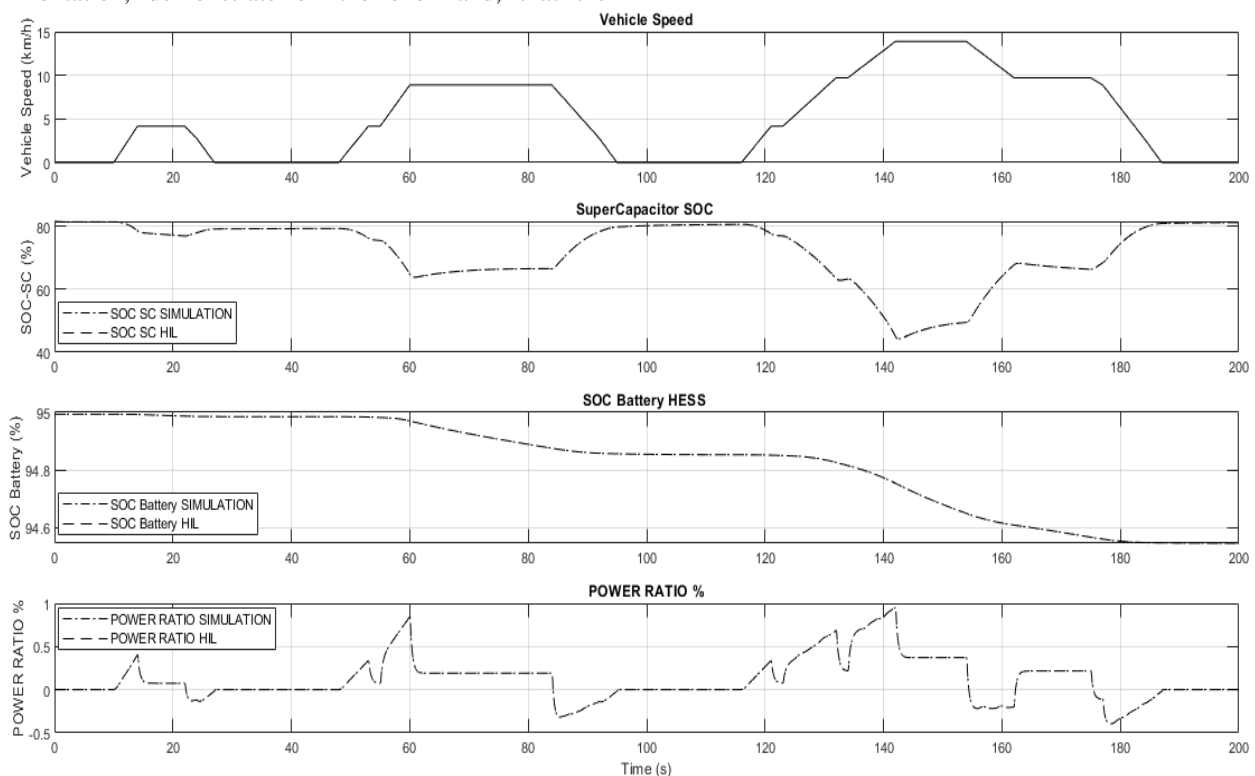


Fig. 13. Simulation results of the EV's HESS under ECE-15 (HIL and simulation results).

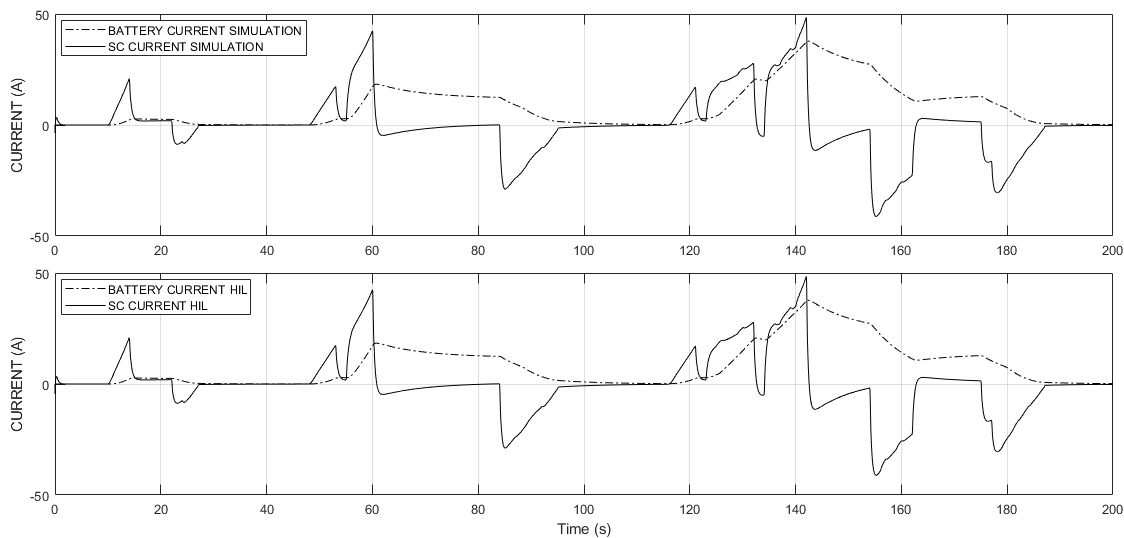


Fig. 14. Battery-SCs currents (HIL and simulation results).

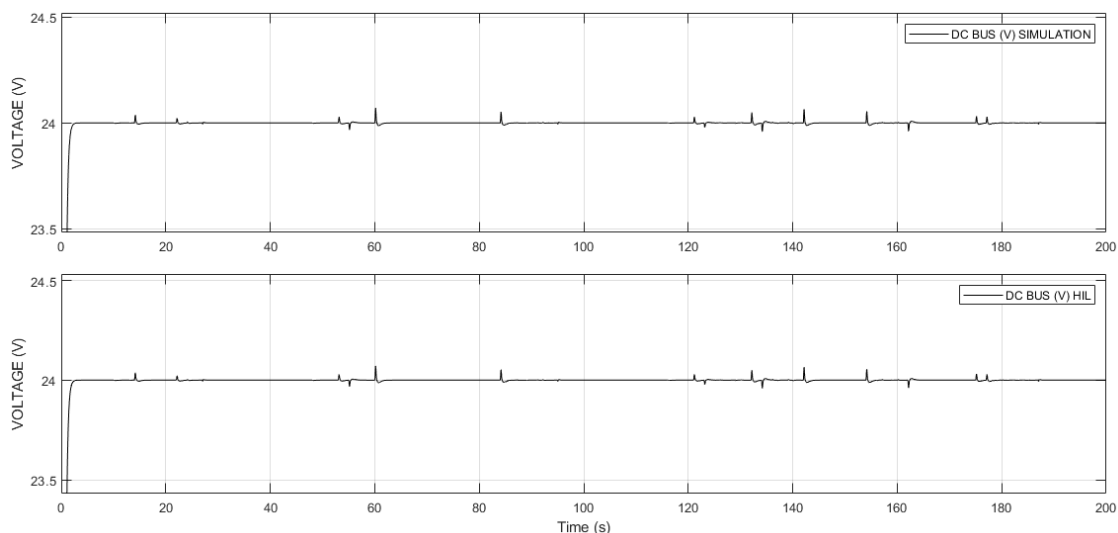


Fig. 15. DC Bus Voltage (HIL and simulation results).

References

- [1] W. Obergassel, O. Lah, and F. Rudolph, “Driving towards transformation? To what extent does global climate governance promote decarbonisation of land transport?” *Earth Syst. Gov.*, vol. 8, p. 100098, Jun. 2021, doi: 10.1016/j.esg.2021.100098.
- [2] W. J. Requia, M. Mohamed, C. D. Higgins, A. Arain, and M. Ferguson, “How clean are electric vehicles? Evidence-based review of the effects of electric mobility on air pollutants, greenhouse gas emissions and human health,” *Atmos. Environ.*, vol. 185, pp. 64–77, Jul. 2018, doi: 10.1016/j.atmosenv.2018.04.040.
- [3] Y. Gai, L. Minet, I. D. Posen, A. Smargiassi, L.-F. Tétreault, and M. Hatzopoulou, “Health and climate benefits of Electric Vehicle Deployment in the Greater Toronto and Hamilton Area,” *Environ. Pollut.*, vol. 265, p. 114983, Oct. 2020, doi: 10.1016/j.envpol.2020.114983.
- [4] P. Spichartz, P. Dost, et C. Sourkounis, “Utilisation of Battery Electric Vehicles and Extended Range Electric Vehicles in a field test,” in *2015 International Conference on Renewable Energy Research and Applications (ICRERA)*, Palermo, Italy, nov. 2015, p. 1168-1173. doi: 10.1109/ICRERA.2015.7418593.
- [5] A. Fotouhi, D. J. Auger, T. Cleaver, N. Shateri, K. Propp, et S. Longo, “Influence of battery capacity on performance of an electric vehicle fleet,” in *2016 IEEE International Conference on Renewable Energy Research and Applications (ICRERA)*, Birmingham, United Kingdom, nov. 2016, p. 928-933. doi: 10.1109/ICRERA.2016.7884471.

- [6] O. Elma, Md. I. Adham, et H. A. Gabbar, "Effects of Ultra-Fast Charging System for Battery Size of Public Electric Bus," in 2020 IEEE 8th International Conference on Smart Energy Grid Engineering (SEGE), Oshawa, ON, Canada, août 2020, p. 142-147. doi: 10.1109/SEGE49949.2020.9182031.
- [7] X. Zhang et al., "A novel quantitative electrochemical aging model considering side reactions for lithium-ion batteries," *Electrochimica Acta*, vol. 343, p. 136070, May 2020, doi: 10.1016/j.electacta.2020.136070.
- [8] S. Yang, Y. Hua, D. Qiao, Y. Lian, Y. Pan, and Y. He, "A coupled electrochemical-thermal-mechanical degradation modelling approach for lifetime assessment of lithium-ion batteries," *Electrochimica Acta*, vol. 326, p. 134928, Dec. 2019, doi: 10.1016/j.electacta.2019.134928.
- [9] F. Savoye, P. Venet, M. Millet, and J. Groot, "Impact of Periodic Current Pulses on Li-Ion Battery Performance," *IEEE Trans. Ind. Electron.*, vol. 59, no. 9, pp. 3481–3488, Sep. 2012, doi: 10.1109/TIE.2011.2172172.
- [10] D. Rimpas et al., "Energy management and storage systems on electric vehicles: A comprehensive review," *Mater. Today Proc.*, p. S2214785321058685, Sep. 2021, doi: 10.1016/j.matpr.2021.08.352.
- [11] Z. Bououchma and J. Sabor, "Online diagnosis of supercapacitors using extended Kalman filter combined with PID corrector," *Int. J. Power Electron. Drive Syst. IJPEDS*, vol. 12, no. 3, p. 1521, Sep. 2021, doi: 10.11591/ijpeds.v12.i3.pp1521-1534.
- [12] R. S. Sankarkumar and R. Natarajan, "Energy management techniques and topologies suitable for hybrid energy storage system powered electric vehicles: An overview," *Int. Trans. Electr. Energy Syst.*, vol. 31, no. 4, Apr. 2021, doi: 10.1002/2050-7038.12819.
- [13] D.-D. Tran, M. Vafaiepour, M. El Baghdadi, R. Barrero, J. Van Mierlo, and O. Hegazy, "Thorough state-of-the-art analysis of electric and hybrid vehicle powertrains: Topologies and integrated energy management strategies," *Renew. Sustain. Energy Rev.*, vol. 119, p. 109596, Mar. 2020, doi: 10.1016/j.rser.2019.109596.
- [14] S. T. Sisakat and S. M. Barakati, "Fuzzy energy management in electrical vehicles with different hybrid energy storage topologies," in 2015 4th Iranian Joint Congress on Fuzzy and Intelligent Systems (CFIS), Zahedan, Iran, Sep. 2015, pp. 1–6. doi: 10.1109/CFIS.2015.7391671.
- [15] S. B. Fahmy, S. E. Guirguis, O. M. Shehata, et E. I. Morgan, "Investigation of an Optimal Charging/Discharging Policy for Electric Vehicles Parking Station in a Smart Grid Environment," in 2020 8th International Conference on Control, Mechatronics and Automation (ICCA), Moscow, Russia, nov. 2020, p. 138-143. doi: 10.1109/ICCA51325.2020.9301484.
- [16] H. Yin, W. Zhou, M. Li, C. Ma, and C. Zhao, "An Adaptive Fuzzy Logic-Based Energy Management Strategy on Battery/Ultracapacitor Hybrid Electric Vehicles," *IEEE Trans. Transp. Electrification*, vol. 2, no. 3, pp. 300–311, Sep. 2016, doi: 10.1109/TTE.2016.2552721.
- [17] H. Jbari, M. Haidoury, R. Askour, and B. Bououlid Idrissi, "Fuzzy Logic Controller for an EV's Dual-Source Hybridization," *E3S Web Conf.*, vol. 297, p. 01039, 2021, doi: 10.1051/e3sconf/202129701039.
- [18] Y. Andika, V. Lystianingrum, and F. A. Pamuji, "Energy Management System Using Cascade Fuzzy for Hybrid Battery and Supercapacitor in Electric Vehicles," in 2021 International Conference on Green Energy, Computing and Sustainable Technology (GECOST), Miri, Malaysia, Jul. 2021, pp. 1–6. doi: 10.1109/GECOST52368.2021.9538648.
- [19] A. Sahbani, K. Cherif and K. Ben Saad, "Multiphase Interleaved Bidirectional DC-DC Converter for Electric Vehicles and Smart Grid Applications," *ijSmartGrid*, 2020, doi: 10.20508/ijsmartgrid.v4i2.102.g86.
- [20] X. Wang, D. Yu, S. Le Blond, Z. Zhao, and P. Wilson, "A novel controller of a battery-supercapacitor hybrid energy storage system for domestic applications," *Energy Build.*, vol. 141, pp. 167–174, Apr. 2017, doi: 10.1016/j.enbuild.2017.02.041.
- [21] H. Hao, X. Guoqing, and Z. Yang, "Hardware-in-the-loop Simulation of Electric Vehicle Powertrain System," in 2009 Asia-Pacific Power and Energy Engineering Conference (APPEEC), Wuhan, China, Mar. 2009, p.5, doi:10.1109/APPEEC.2009.4918397.
- [22] R. Morello et al., "Hardware-in-the-loop simulation of FPGA-based state estimators for electric vehicle batteries," in 2016 IEEE 25th International Symposium on Industrial Electronics (ISIE), Santa Clara, CA, USA, Jun. 2016, pp. 280–285. doi: 10.1109/ISIE.2016.7744903.
- [23] J. J. Rodriguez-Andina, M. D. Valdes-Pena, and M. J. Moure, "Advanced Features and Industrial Applications of FPGAs—A Review," *IEEE Trans. Ind. Inform.*, vol. 11, no. 4, pp. 853–864, Aug. 2015, doi: 10.1109/TII.2015.2431223.
- [24] J. M. Blanes, R. Gutierrez, A. Garrigos, J. L. Lizan, and J. M. Cuadrado, "Electric Vehicle Battery Life Extension Using Ultracapacitors and an FPGA Controlled Interleaved Buck–Boost Converter," *IEEE Trans. Power Electron.*, vol. 28, no. 12, pp. 5940–5948, Dec. 2013, doi: 10.1109/TPEL.2013.2255316.
- [25] V. Shende, K. V. Singh, H. O. Bansal, and D. Singh, "Sizing Scheme of Hybrid Energy Storage System for Electric Vehicle," *Iran. J. Sci. Technol. Trans. Electr. Eng.*, vol. 45, no. 3, pp. 879–894, Sep. 2021, doi: 10.1007/s40998-021-00416-x.
- [26] M. V. Chung, D. T. Anh, P. Vu, and L. M. Nguyen, "Hardware in the loop co-simulation of finite set-model predictive control using FPGA for a three level CHB inverter," *Int. J. Power Electron. Drive Syst. IJPEDS*, vol.

- 11, no. 4, p. 1719, Dec. 2020, doi: 10.11591/ijpeds.v11.i4.pp1719-1730.
- [27] A. Bouscayrol, P. Delarue, X. Guillaud, W. Lhomme, and B. Lemaire-Semail, "Simulation of a Wind Energy Conversion System using Energetic Macroscopic Representation," in 2012 15th International Power Electronics and Motion Control Conference (EPE/PEMC), Novi Sad, Serbia, Sep. 2012, p. DS3e.8-1-DS3e.8-6. doi: 10.1109/EPEPEMC.2012.6397362.
- [28] F. Giraud, A.-L. Allegre, A. Bouscayrol, K. Chen, B. Lemaire-Semail, and W. Lhomme, "Project-based teaching unit using energetic macroscopic representation to design drive controllers," in 2010 IEEE Vehicle Power and Propulsion Conference, Lille, France, Sep. 2010, pp. 1–6. doi: 10.1109/VPPC.2010.5729099.